DOI: 10.18462/iir.gl2024.1188

# Comparative study of heat storage system in water vapor compression heat pump for industrial processes

**Seon Tae KIM*[(a)], Steffen KLÖPPEL[(a)], Eberhard NICKE[(a)], K. MALLESWARARAO[(b)], Marc LINDER[(b)], Panagiotis STATHOPOULOS[(a)]**

(a) Institute of Low-Carbon Industrial Process, German Aerospace Center (DLR), Mandau-Höfe, Äußere Oybiner Straße 14/16, Zittau 02763, Germany, * seon.kim@dlr.de

(b) Institute of Engineering Thermodynamics, German Aerospace Center (DLR), Pfaffenwaldring 38–40, Stuttgart, 70569, Germany

## ABSTRACT

The thermodynamic performance of a two-stage high-temperature heat pump (HTHP), utilizing water/steam as a refrigerant, along with two distinct thermal energy storage systems, concrete sensible heat storage (SHS) and strontium bromide/water thermochemical energy storage ($SrBr_2/H_2O$ TCES), were evaluated. The proposed HTHP demonstrated sufficient capability to supply heat above 200°C with a high COP of 5.2-7.5. While concrete SHS cannot release heat beyond the temperature at which it was stored, 190°C, TCES can release heat above 200°C. Additionally, the SHS system cannot satisfy the limited heat release operation time when it has a lower cycle out temperature than the condensation temperature of the HTHP cycle. It was also observed that $SrBr_2/H_2O$ TCES required 45% less material mass and 68% less volume, respectively. In the techno-economic evaluation, the integrated system comprising HTHP and TCES yielded a net present value of €454,075-€171,890. Furthermore, the internal rate of return was calculated to be between 15.3-23.0%.

Keywords: Water/steam (R-718) Refrigerant, High-temperature Heat Pump, Thermal Energy Storage, Sensible Heat Storage, Thermochemical Energy Storage, Techno-economic Analysis

## 1 INTRODUCTION

Global greenhouse gas (GHG) emissions have continued to increase over the last decades. Specifically, carbon dioxide ($CO_2$) emissions, which are a major contributor to global warming, were estimated at approximately 36.8 Gt in 2022. The industrial sector is responsible for approximately 35% of global GHG emissions when reallocated to the final energy consumption sectors. Among the various energy services in the industry, thermal energy demand is dominant in the industrial sector with specific temperature levels of each subsector, and it has the largest potential for increasing the electrification rate. In particular, heat pumps offer significant potential across various sectors and can play an important role in decarbonizing industrial heat production below 200°C, swiftly reducing reliance on fossil fuels.

From this perspective, the deployment of industrial heat pumps utilizing renewable electricity holds significant importance in achieving authentic carbon emission reduction through the electrification of industrial processes. Additionally, with the increasing adoption of industrial high-temperature heat pumps (HTHP) and the utilization of renewable energy, an accompanying rise in the imbalance between supply and demand is anticipated, necessitating the development of storage technology.

The current study investigates the performance of a two-stage water vapor (R-718) HTHP capable of delivering heat at approximately 200°C, along with two distinct thermal energy storage (TES) systems: sensible heat storage (SHS), which is widely used at a high technical readiness level (TRL) for high temperatures, and thermochemical energy storage (TCES), which has higher energy density and can flexibly control storage and discharge levels. From a thermodynamic perspective, the potential of the HTHP and TCES systems to replace the existing SHS system will is evaluated.

## 2 SYSTEM MODELING

### 2.1 Multistage water vapor compression cycle

A two-stage water vapor compression cycle with intercooling was introduced as the HTHP cycle, as shown in Fig. 1. The working fluid, water/steam, undergoes compression to an intermediate pressure and is subsequently cooled near its condensation temperature. The resulting slightly superheated steam is then recompressed to the condensation pressure. The International Association for the Properties of Water and Steam, utilizing the industrial formulation 1997 (IAPWS-IF97), was adopted for calculating the properties of water/steam in the HTHP cycle.

A two-stage water vapor compression cycle with intercooling was introduced, as shown in Fig. 1. The evaporation temperature, $T_{evap}$, was set at 100°C, and the condensation temperature, $T_{cond}$, varies to 130, 140, 150 and 160°C, respecting a temperature lift limitation of 60-65 K when the pressure ratio of each stage is below 2.5. The intermediate pressure was determined to have the same pressure ratio between the first and second stages to achieve the highest coefficient of performance (COP). The heat sink flow was designed to provide consistent thermal energy to the TES systems and recover it. This flow operates at the same pressure as condenser and maintains a constant mass flow rate during both the storage and release operation of the TES system. During the storage operation, the HTHP supplies thermal energy of 500 kW at 200°C for 8 hours, with a maximum heat release operation duration of 16 hours. Additionally, it was assumed that all the temperature differences between the hot and cold sides after heat exchangers were 10 K.

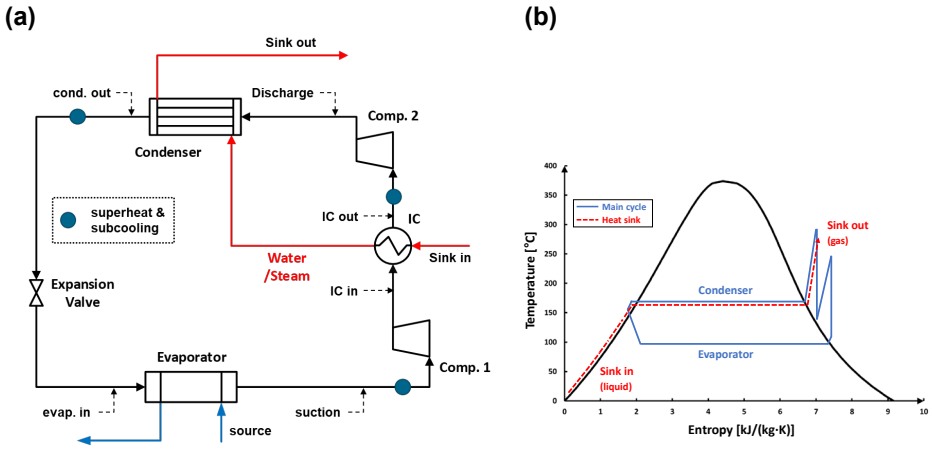


**Figure 1: Image of (a) Schematic diagram of the HTHP cycle and (b) *T-S* diagram**

### 2.2 Thermal energy storage system

The SHS method is widely used and represents the most common type of TES technology. In the current study, concrete is considered as the SHS storage medium due to its ability to withstand cyclic stress at temperatures up to 500°C over extended lifetimes. This concrete SHS system is configured as a pumped thermal energy storage system with two tanks, utilizing air as the heat transfer fluid (HTF). Operational strategies are illustrated in Fig. 2. During the storage mode, low-temperature air at $T_{amb}$ = 25°C in the cold tank is heated by high-temperature steam generated from the HTHP and transferred to the hot tank over 8 hours. In the heat release operation, high-temperature air transfers heat to low-temperature water/steam in the heat sink flow, which is then stored in the cold tank. The heat release operation is limited to a maximum of 16 hours, assuming the TES system can complete at least one cycle per day. The specifications of the SHS system were calculated based on the properties of concrete at 200°C, as detailed in Table 1.

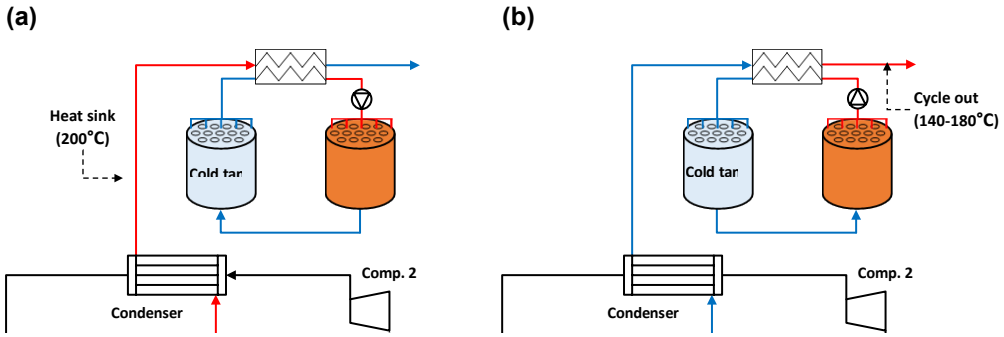


**Figure 2: Image of the sensible heat storage system: (a) Heat storage operation and (b) Heat release operation**

**Table 1. Properties of concrete at 200°C for SHS system**

| Specific heat capacity, *Cp* [J/(kg K)] | Density, *ρ* [kg/m3] | Thermal conductivity, *λ* [W/(m K)] |
|---|---|---|
| 903 | 2250 | 1.60 |

Among the various reversible chemical reactions, the strontium bromide and water ($SrBr_2/H_2O$) working pair has been selected for the TCES system. This reaction exhibits high specific power at temperatures above 150°C and has gained attention as a promising material for storing heat within the temperature range of 150-300°C. The $SrBr_2$ monohydrate, $SrBr_2{\cdot}H_2O$, can store heat through dehydration, while the hydration of anhydrous $SrBr_2$ releases heat, Eq. (1).

$$SrBr_2(s) + H_2O(g) \rightleftarrows SrBr_2 \cdot H_2O(s) \qquad \Delta H = 71.98\ kJ/mol \qquad \text{Eq. (1)}$$

The operational schematic diagram of the TCES system with a packed bed reactor is illustrated in Fig. 3. During the heat storage operation, the dehydration of $SrBr_2{\cdot}H_2O$ is initiated by a heat sink at 200°C, and the resulting water vapor condenses in a water reservoir at 35°C. Unlike the SHS system, the TCES system can control the cycle out temperature, $T_{\text{cycle out}}$, by regulating the hydration temperature corresponding to the hydration pressure. Additionally, Table 2 shows the molar mass, *M*, and density, *ρ*, of anhydrous and monohydrate $SrBr_2$.

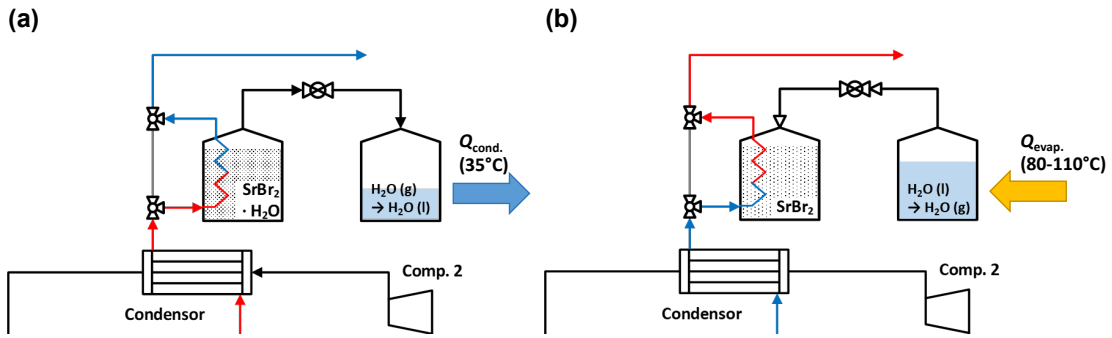


**Figure 3: Image of thermochemical energy storage: (a) Heat storage operation and (b) Heat release operation**

**Table 2. Properties of $SrBr_2$ ($SrBr_2{\cdot}H_2O$) for TCES system**

| Materials | Molar mass, *M*, [g/mol] | Density, *ρ*, [kg/m$^3$] | Enthalpy of hydration, Δ*H*, [kJ/mol] |
|---|---|---|---|
| $SrBr_2$ | 247.43 | 4216 | 71.98 |
| $SrBr_2{\cdot}H_2O$ | 265.43 | 3911 | |

### 2.3 Economic model

The economic feasibility of HTHP compared to hot water boilers (HWB) has been assessed based on their suitability as heat sources for the TES system. The economic analysis spans, *n*, a period of 20 years with a discount rate, *d*, of 3.5% and an inflation rate, *i*, of 2.8%. The net present value (NPV) was calculated using Eq. (2), and the internal rate of return (IRR) is determined by setting the NPV = 0 and solving for the discount rate, *d*.

$$NPV = -INV + \sum_{n=1}^{n=20} \frac{CF_n \cdot (1+i)^{n-1}}{(1+d)^n} \quad \text{Eq. (2)}$$

where *i* represents the inflation rate, *n* denotes the number of time periods, $CF_n$ is the annual net saving electricity cost at the year, *n*, and INV represents the initial investment for the respective systems.

The initial cost of the HTHP system comprises two stages, two sets of turbomachinery and related components. Only the cost of the storage medium for the TES system is considered, as the expenses of other TES components can vary significantly depending on the configuration. $CF_n$ is derived from the difference in required electricity between HWB and HTHP, calculated based on system efficiency. Cost information for the HTHP system, provided by manufacturers according to our specifications, and the storage medium for TES systems are summarized in Table 3.

**Table 3. Cost information for HTHP and storage medium of TES systems**

| System | Components | Cost | Unit |
|---|---|---|---|
| HTHP | Compressor | 88,000 | [€] |
| | Gear box | 72,000 | [€] |
| | Electrical motor | 6,700 | [€] |
| | Evaporator | 34,800 | [€] |
| | Condenser | 17,345 | [€] |
| | Intercooler | 8,000 | [€] |
| TES | Concrete | 1.36 | [€/$kW_{th}$] |
| | $SrBr_2$ ($SrBr_2 \cdot H_2O$) | 0.52 | [€/$kW_{th}$] |

## 3 PERFORMANCE EVALUATION

### 3.1 High-temperature heat pump (HTHP) cycle

The performance of HTHP cycle under different temperature conditions was evaluated by determining the overall thermodynamic properties, such as pressure, temperature, and enthalpy at each point of the cycle using thermodynamic heat and energy balances for the multistage high-temperature heat pump. The important parameters, including the mass flow rate of the HTHP main cycle and the power consumption of the two compressors, were estimated using Eqs. (3) and (4). Additionally, the coefficient of performance (COP) and thermodynamic efficiency, $\eta_{carnot}$, of the HTHP cycle were defined using Eqs. (5) and (6). These calculations were based on the thermal energy obtained from the condenser and intercooler (IC), as well as the calculated work input for the compressor, $W_{comp}$.

$$\dot{m}_{main} = \frac{\dot{Q}_{sink}}{((H_{IC\ out} - H_{IC\ in}) - (H_{dis} - H_{cond\ out}))} \quad \text{Eq. (3)}$$

$$W_{comp} = \left(\frac{(H_{IC\ in} - H_{suc}) \times \dot{m}_{main}}{\eta_{mech.}}\right) + \left(\frac{(H_{dis} - H_{IC\ out}) \times \dot{m}_{main}}{\eta_{mech.}}\right) \quad \text{Eq. (4)}$$

$$COP = \dot{Q}_{sink} / W_{comp} \quad \text{Eq. (5)}$$

$$\eta_{carnot} = \frac{COP}{COP_{Carnot}} \quad \text{Eq. (6)}$$

According to the assumption in previous section, the mass flow rate of the heat sink flow, $\dot{m}_{\mathrm{sink}}$, is assumed to remain constant for both the heat storage and release opertions, and it is assumed to have the same pressure as $P_{\mathrm{dis}}$ of the main cycle. It was calculated based on the capacity of water/steam and the enthalpy of vaporization at the respective $T_{\mathrm{cond}}$.

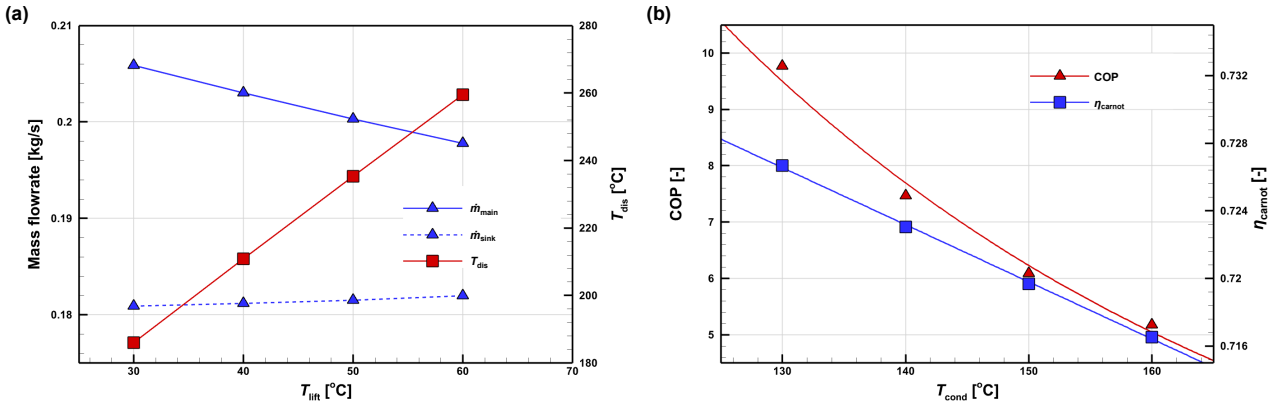


**Figure 4: Performance of HTHP with $T_{\mathrm{evap}}$ = 100°C: (a) Mass flow rates and discharge temperature by $T_{\mathrm{lift}}$ and (b) COP and Thermodynamic efficiency by $T_{\mathrm{cond}}$.**

The changes in mass flow rate of the main and heat sink, $\dot{m}_{\mathrm{main}}$ and $\dot{m}_{\mathrm{sink}}$, by temperature lift, $T_{\mathrm{lift}}$, are shown in Fig. 4(a). Overall, $\dot{m}_{\mathrm{main}}$ decreases as $T_{\mathrm{lift}}$ increases, reflecting the enthalpy differences between the inlet and outlet of the intercooler and condenser. However, $\dot{m}_{\mathrm{sink}}$ remains relatively constant because $\dot{Q}_{\mathrm{sink}}$ is fixed at 500 kW, and the specific heat capacity and enthalpy of vaporization do not vary with temperature. Regarding $T_{\mathrm{dis}}$, it increases with $T_{\mathrm{lift}}$ and is predominantly influenced by $T_{\mathrm{lift}}$ rather than other parameters. In particular, a minimum $T_{\mathrm{lift}}$ of 40°C is required to supply heat of 200°C to the TES system during storage operation.

The COP and $\eta_{\mathrm{carnot}}$, of the two-stage HTHP cycle are shown in Fig. 4 (b). The overall COP values decrease exponentially with $T_{\mathrm{lift}}$, whereas $\eta_{\mathrm{carnot}}$ values decrease proportionally. Given that a minimum $T_{\mathrm{lift}}$ of 40°C is necessary to provide heat above 200°C, the COP of the HTHP cycle ranges from 5.2-7.5, while $\eta_{\mathrm{carnot}}$ is approximately 0.72.

## 3.2 Thermal energy storage systems

### 3.2.1 Sensible heat storage (SHS) system

In storage operation, the HTHP cycle supplies 500 kW of heat continuously for 8 hours, storing a total thermal energy of 14,400 MJ in both TES systems without any heat loss. The temperature of the heat transfer fluid (HTF) was maintained 10 K below the heat sink outlet temperature of 200°C. The required air flow rate for the storage operation, calculated using Eq. 7, is $\dot{m}_{\mathrm{air,stor}} = 2.82\ \mathrm{kg/s}$. During the heat release operation, the SHS system can achieve various cycle outlet temperatures, $T_{\mathrm{cycle\ out}} < T_{\mathrm{stor}} - 10$ K, by controlling the heat output rate $\dot{Q}_{\mathrm{SHS,rel}}$. The required $\dot{Q}_{\mathrm{SHS,rel}}$ for each target $T_{\mathrm{cycle\ out}}$ can be determined from the enthalpy balance of the heat sink flow. The corresponding mass flow rates of air, $\dot{m}_{\mathrm{air,rel}}$, In the SHS system, the calculations are calculated using Eq. 8. Additionally, unlike the TCES system, the operation of the SHS system involves the use of an air pump to deliver heat continuously.

$$\dot{m}_{air,stor} = \dot{Q}_{sink} / \left( c_{p_{air\ at\ 190°C}} \times (T_{stor} - T_{amb}) \right) \quad \text{Eq. (7)}$$

$$\dot{m}_{sink} \times \left( H_{T_{cycle\ out}} - H_{amb} \right) = \dot{Q}_{SHS,rel} = \dot{m}_{air,rel} \times \left( T_{stor} - T_{cycle\ out} \right) \quad \text{Eq. (8)}$$

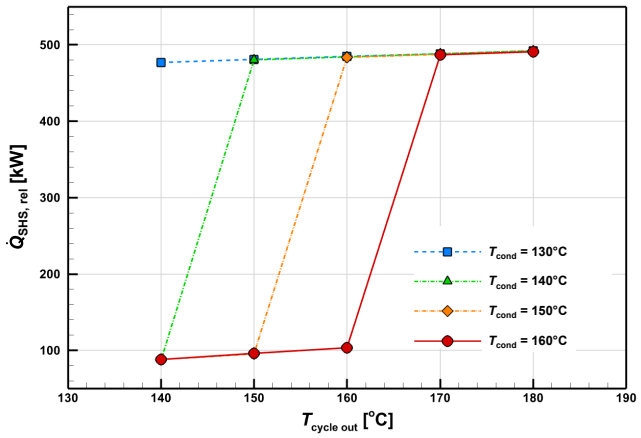


**Figure 5: Heat output rate, $\dot{Q}_{SHS,rel}$, of the SHS system**

The heat output rate, $\dot{Q}_{\mathrm{SHS,rel}}$, varies during the heat release operation depending on the targeted cycle outlet temperature, Fig. 5. Since the heat sink flow maintains the same pressure as the discharge pressure of the HTHP main cycle, $P_{dis}$, it maintains a consistent condensation temperature through heat release. The enthalpy of the heat sink flow increases sharply above the condensation temperature, resulting in a significant increase in both $\dot{Q}_{\mathrm{SHS,rel}}$ and $\dot{m}_{\mathrm{air,rel}}$ when the targeted temperature exceeds the condensation temperature.

### 3.2.2 Thermochmeical energy storage (TCES) system

The Gibbs free energy change of a reaction, $\Delta G$, is obtained from the reaction enthalpy change, $\Delta H$, and the entropy change, $\Delta S$, as shown in Eq. 9.

$$\Delta G = \Delta H - T\Delta S \qquad \text{Eq. (9)}$$

where $\Delta G$ has the following relationship with the reaction equilibrium constant, $K_{eq}$, for the solid-gas reaction assuming ideal gas properties. The reversible reaction condition is established at around $K_{eq}$ = 1 and the linear form of the Van't Hoff plot is derived from Eq. 10, and Fig. 6 shows the Van't Hoff diagram of $SrBr_2/H_2O$ solid-gas system. The TCES system can store heat through dehydration at a specific temperature, $T_{dehy}$, and achieve a higher output temperature than dehydration temperature, $T_{hyd} > T_{dehy}$, by controlling hydration pressure. Therefore, the heat release operation of the TCES system is also referred as the temperature upgrade operation of a chemical heat pump.

$$ln\, K_{eq}(T,P) = ln\left(\frac{P}{P^0}\right) = \frac{\Delta G}{RT} = -\frac{\Delta H}{RT} + \frac{\Delta S}{R} \qquad \text{Eq. (10)}$$

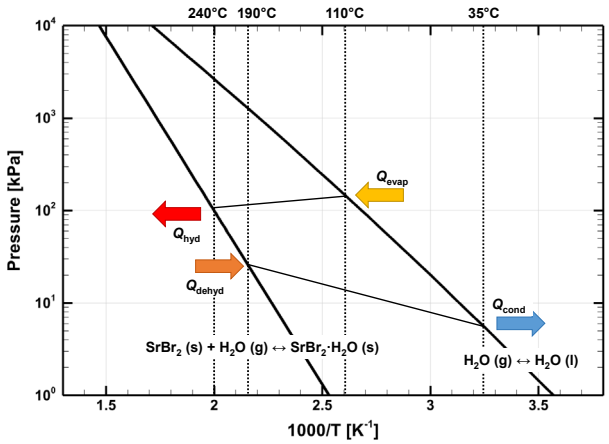


**Figure 6: Van't Hoff diagram for the $SrBr_2/H_2O$ TCES system**

In this study, during the heat storage operation, monohydrous $SrBr_2$ was decomposed at 190°C, and the resulting water vapor was condensed at 35°C. The evaporation temperature, $T_{evap}$, was limited to 110°C, as waste heat from the industrial process was utilized for evaporation. Therefore, four different evaporation temperatures were selected, $T_{evap}$ = 80, 90, 100, and 110°C. The hydration temperatures were calculated as $T_{hyd}$ = 206, 217, 227, and 238°C, respectively, corresponding to the saturated water vapor pressure at these temperatures.

### 3.2.3 Comparison of both TES systems

The heat output rate and operable heat release time of both TES systems are compared in Fig. 7. Generally, the TCES system exhibits higher heat output rate and cycle outlet temperature, $\dot{Q}_{\mathrm{rel}}$ and $T_{\text{cycle out}}$, than the SHS system, as shown in Fig. 7(a). Due to the stored thermal energy temperature in the SHS system, $T_{\text{SHS stor}}$, being 190°C, the maximum cycle outlet temperature, $T_{\text{cycle out}}$, during heat release operation for the SHS system is constrained to 180°C. In contrast, the $T_{hyd}$ of the TCES system, obtained from the equilibrium pressure in Eq. 10, exceeds 200°C, allowing an expected $T_{\text{cycle out}}$ higher than 196°C. Furthermore, when $T_{\text{cycle out}}$ of the SHS TES system is lower than $T_{cond}$, $\dot{Q}_{\mathrm{rel}}$ is low. Despite both TES systems storing the same amount of heat, 14,400 MJ, the available heat release time, $\tau_{\mathrm{rel}}$, differs. The SHS system with a $T_{\text{cycle out}}$ lower than $T_{cond}$, can operate for more than 35 hours because $\dot{m}_{sink}$ is fixed throughout heat storage and heat release operations. From the perspectives of heat release operation of the HTHP system mentioned in section 2.1, the SHS system with a $T_{\text{cycle out}}$ lower than $T_{cond}$ cannot meet the heat release operation time, $\tau_{\mathrm{rel}}$ < 16 hours, unlike under other conditions, Fig. 7(b).

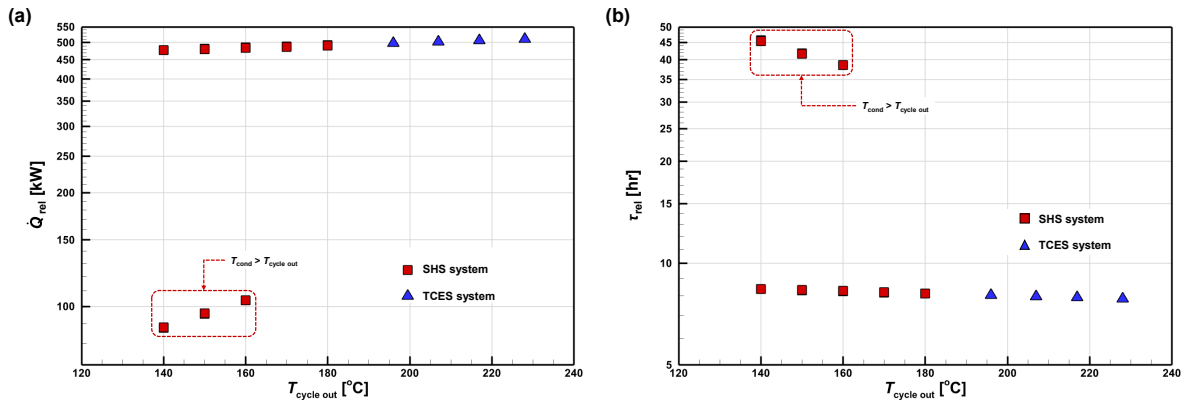


**Figure 7: Performance comparison of thermal energy storage systems: (a) Heat output rate, $\dot{Q}_{\mathrm{rel}}$, and (b) Heat release time, $\tau_{\mathrm{rel}}$**

Based on the physical properties in Table 1 and 2, the required amount and volume of thermal energy storage materials are obtained, Table 4. In comparison to a concrete SHS system, the $SrBr_2/H_2O$ TCES system only requires 45% and 68% less mass and volume for storage operation.

**Table 4. Specifications of TES systems**

| | SHS | TCES | Note |
|---|---|---|---|
| Material | Concrete | $SrBr_2 \cdot H_2O$ | TCES/SHS |
| Weight, *m* [kg] | 96,648 | 53,101 | 0.55 |
| Volume, *V* [$m^3$] | 43.0 | 13.6 | 0.32 |

## 4 TECHNO-ECONOMIC ANALYSIS

The net present value (NPV) of the integrated HTHP and TCES system, compared to hot water boilers (HWB) using natural gas, was conducted over a 20-year lifespan. A positive NPV indicates the integrated system's cost effectiveness, with the relationship between NPV, discount rate, *d*, and COP shown in Fig.

8(a). The COP range was constrained to 4.5-7.5 as HTHP systems with COPs exceeding 7.5 could not supply heat at 200°C to the TES system. NPV is more sensitive to changes in discount rate than to COP variations. For COPs of 7.5 and 4.5, the integrated system yields NPVs of €454,075 and €171,890, respectively. The internal rate of return (IRR), calculated by setting NPV = 0 in Eq. 2 and solving for the discount rate, *d*, is shown in Fig. 8(b). An IRR higher than the investor's required rate of return indicates the viability of the investment. The HTHP and TCES integrated system shows an IRR variation of 15.3-23.0%.

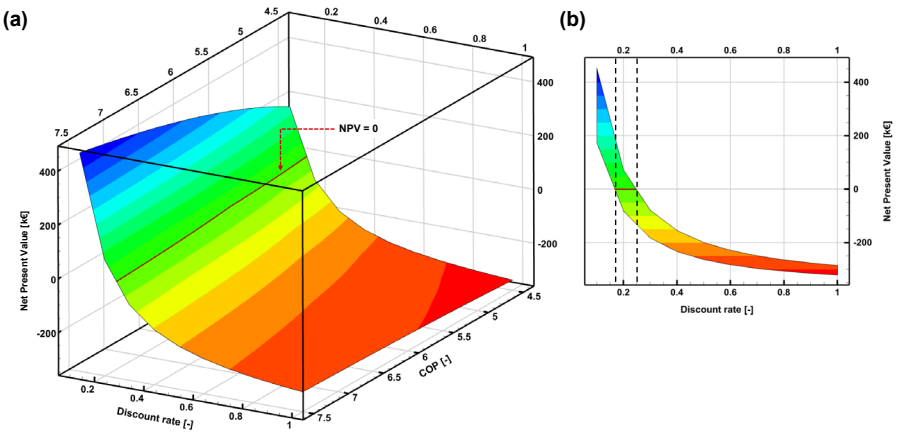


**Figure 8: NPV of the integrated system, HTHP and TCES, at different discount rates and COPs**

## 5 CONCLUSIONS

In the present work, an integrated system combining HTHP and TES system was proposed as a replacement for existing fossil fuel boilers, investigated from both thermodynamic and techno-economics perspectives. The multi-stage water vapor HTHP with high COP, demonstrated effective capability in reducing $CO_2$ emissions from industrial processes. However, conflicting thermodynamic results were observed between the two proposed TES systems. The TCES system, characterized by its higher energy density and ability to discharge heat at temperatures higher than those at which it was stored, shows promising potential for high-temperature industrial applications. Techno-economic analyses were also conducted to compare the integrated HTHP and TCES system with the existing natural gas boiler.

As a further study, extensive techno-economic evaluation and optimization of the integrated HTHP and TCES system will be conducted. The study will encompass comprehensive assessments, including levelized cost and consideration of transient boundary conditions.

## NOMENCLATURE

| | | | |
|---|---|---|---|
| $C_p$ | specific heat capacity (J/kg$^{-1}$×K$^{-1}$) | $Q$ | heat transfer (kJ) |
| *CF* | cash flow (€) | R | molar gas constant (8.314472 J×mol$^{-1}$×K$^{-1}$) |
| G | Gibbs free energy (kJ×mol$^{-1}$) | $S$ | entropy (kJ×K$^{-1}$) |
| $H$ | enthalpy (kJ×kg$^{-1}$×K$^{-1}$) | $T$ | temperature (K) |
| $i$ | Inflation rate (%) | $V$ | volume (m$^3$) |
| $m$ | mass (kg) | $\eta_{carnot}$ | Carnot efficiency (-) |
| $n$ | life span (years) | $\tau$ | time (sec) |
| $P$ | pressure (kPa) | | |

## REFERENCES


Lamb, W.F., Wiedmann T., Pongratz J., Andrew R., Crippa M., Olivier, J.G.J., et al., 2021. A review of trends and drivers of greenhouse gas emissions by sector from 1990 to 2018, Environ. Res. Lett. 16(7), 73005.

Fleitern, T., Jan, S., Mario, R., Andreas, M., Lukas, K., Marcus, H., et al., 2016. Mapping and analyses of the current and future (2020-2030) heating/cooling fuel deployment (fossil/renewables) Work package 1: Final energy consumption for the year 2012 Final report, 54296.

Tong, D., Farnham, D.J., Duan, L., Zhang, Q., Lewis, N.S., Caldeira, K., et al., 2016. Geophysical constraints on the reliability of solar and wind power worldwide, Nature communications 12(1), 6146.

Kim, S.T., Hegner, R., Özuylasi, G., Stathopoulos, P., Nicke, E., 2023. Performance analysis of multistage high-temperature heat pump cycle, Energy Science & Engineering 11(10), 3500-3511.

Laing, D., Lehmann, D., Fiß, M., Bahl, C., 2009. Test Results of Concrete Thermal Energy Storage for Parabolic Trough Power Plants, Journal of Solar Energy Engineering 131(4), 041007.

Pan, J., Zou, R., Jin, F., 2017. Experimental Study on Specific Heat of Concrete at High Temperatures and Its Influence on Thermal Energy Storage, Energies 10(1), 33.

Anderberg, Y., 1991. Consequence analysis of Eurocode 2 (design of concrete structures), part 10, structural fire design (draft April 1990). Fire Safety Design, Lund.

Stengler, J., Bürger, I., Linder, M., 2020. Thermodynamic and kinetic investigations of the SrBr2 hydration and dehydration reactions for thermochemical energy storage and heat transformation, Applied Energy 277, 115432.

Perry, D.L., 2011. Handbook of Inorganic Compounds. CRC Press, Boca Raton.

Strasser, M.N., Selvam, R.P., 2014. A cost and performance comparison of packed bed and structured thermocline thermal energy storage systems. Solar Energy 10, 390–402.

Gilles, D., Segato, T., Courbon, E., Degrez, M., D'Ans, P., 2018. Affordable Process for the Production of Strontium Bromide Used in Low Grade Heat Recovery Applications, Procedia CIRP 69, 383–288.

Jovet, Y., Lefèvre, F., Laurent, A., Clausse, M., 2022. Combined energetic, economic and climate change assessment of heat pumps for industrial waste heat recovery, Applied Energy 313, 118854.